

Surface ocean cooling in the Eocene North Atlantic coincides with declining atmospheric CO₂

Gordon N. Inglis¹, Rehemat Bhatia², David Evans¹, Jiang Zhu³, Wolfgang Müller⁴, David Matthey⁵, David Thornalley², Richard Stockey⁶, and Bridget Wade²

¹University of Southampton

²University College London

³National Center for Atmospheric Research

⁴Unknown

⁵Royal Holloway University

⁶School of Ocean and Earth Science

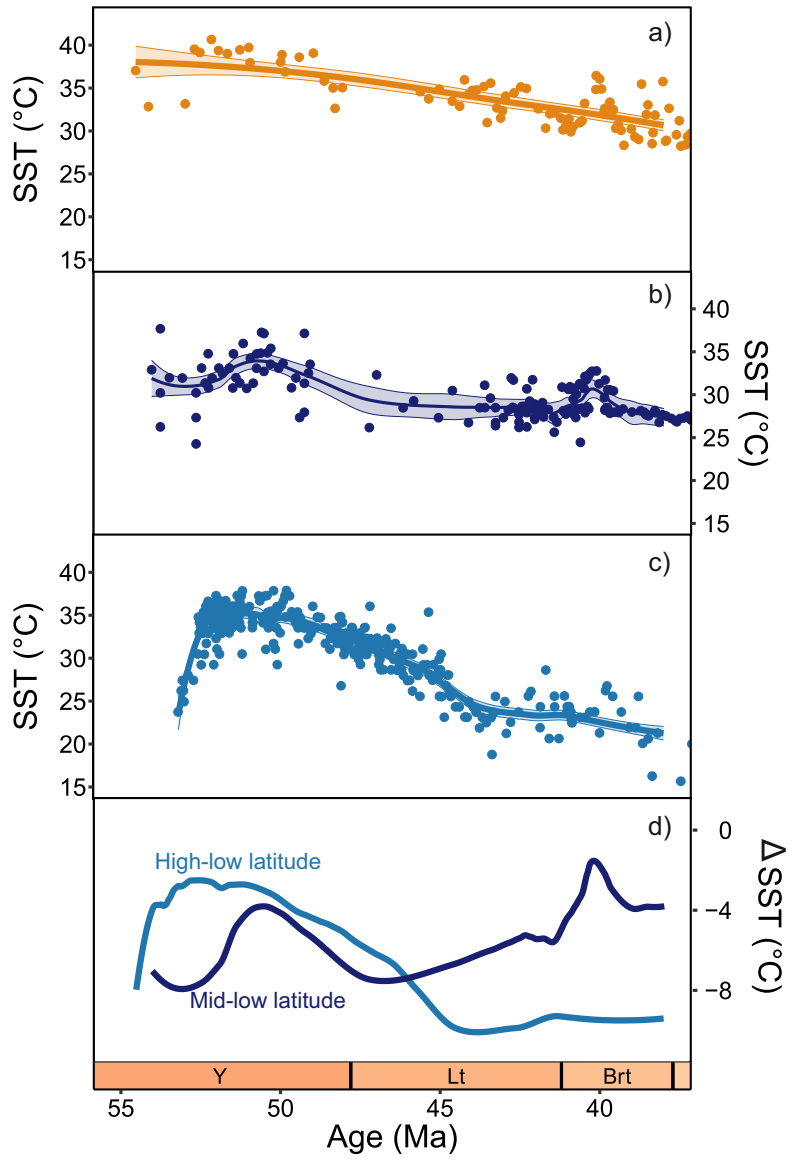
August 1, 2023

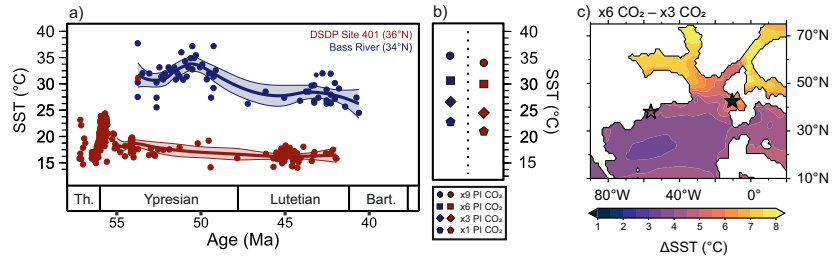
Abstract

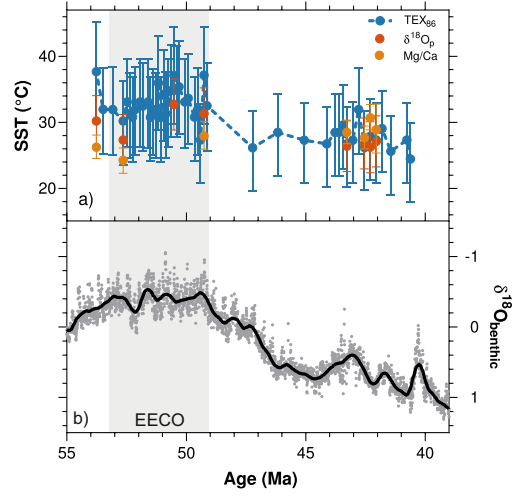
The Eocene (56–34 million years ago) is characterised by declining sea surface temperatures (SSTs) in the low latitudes (~4°C) and high southern latitudes (~8–11°C), in accord with decreasing CO₂ estimates. However, in the mid-to-high northern latitudes there is no evidence for surface water cooling, suggesting thermal decoupling between northern and southern hemispheres and additional non-CO₂ controls. To explore this further, we present a multi-proxy (Mg/Ca, δ¹⁸O, TEX86) SST record from the western North Atlantic (~36°N paleolatitude). Our data confirm a long-term decline in SSTs of ~5°C between the early (~53 Ma) and the middle (~42 Ma) Eocene, supporting declining atmospheric CO₂ as the primary mechanism of Eocene cooling. However, from the middle Eocene onwards, North Atlantic zonal temperature gradients are decoupled, which we attribute to the incursion of warmer waters into the eastern North Atlantic and the inception of Northern Component Water across the early-middle Eocene transition.

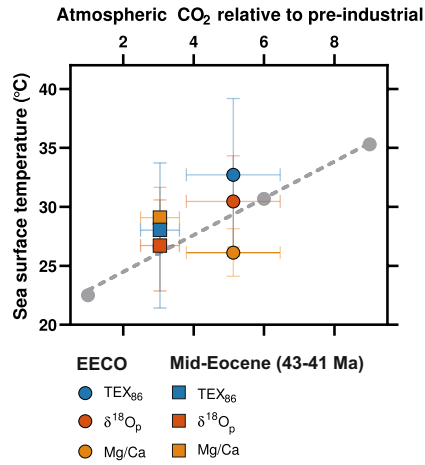
Hosted file

968568_0_art_file_11208806_ryxxgp.docx available at <https://authorea.com/users/544012/articles/656717-surface-ocean-cooling-in-the-eocene-north-atlantic-coincides-with-declining-atmospheric-co2>









Hosted file

968568_0_supp_11180025_ry3fzr.docx available at <https://authorea.com/users/544012/articles/656717-surface-ocean-cooling-in-the-eocene-north-atlantic-coincides-with-declining-atmospheric-co2>

1 **Surface ocean cooling in the Eocene North Atlantic coincides with**
2 **declining atmospheric CO₂**

3
4 Gordon N. Inglis* ⁽¹⁾, Rehemat Bhatia* ⁽²⁾, David Evans ^(1,3), Jiang Zhu⁽⁴⁾, Wolfgang Müller ⁽³⁾, David
5 Mattey ⁽⁵⁾ David Thornalley ⁽⁶⁾, Richard G. Stockey ⁽¹⁾, Bridget S. Wade ⁽²⁾

6
7 (1) School of Ocean and Earth Science, University of Southampton, UK

8 (2) Department of Earth Sciences, University College London, UK

9 (3) Institute of Geosciences, Goethe University Frankfurt, Frankfurt, Germany

10 (4) National Center for Atmospheric Research, Colorado, USA

11 (5) Department of Earth Sciences, Royal Holloway University of London (RHUL), UK

12 (6) Department of Geography, UCL, UK

13
14 * contributed equally to this work

15 Corresponding author: Gordon N. Inglis

16 Email: gordon.inglis@soton.ac.uk. Telephone: +44 (0)117 954 6395

17
18
19
20
21
22
23
24
25
26
27

28 **Key points:**

- 29 • Long-term decline in North Atlantic sea surface temperatures ($\sim 5^\circ\text{C}$) between the early
30 ($\sim 53\text{ Ma}$) and the middle ($\sim 42\text{ Ma}$) Eocene.
- 31 • This indicates that CO_2 was likely responsible for the onset of long-term Eocene cooling.
- 32 • However, zonal temperature gradients in the North Atlantic appear decoupled due to
33 inception of Northern Component Water formation.

34

35 **Abstract:**

36 The Eocene (56–34 million years ago) is characterised by declining sea surface temperatures
37 (SSTs) in the low latitudes ($\sim 4^\circ\text{C}$) and high southern latitudes ($\sim 8\text{--}11^\circ\text{C}$), in accord with decreasing
38 CO_2 estimates. However, in the mid-to-high northern latitudes there is no evidence for surface
39 water cooling, suggesting thermal decoupling between northern and southern hemispheres and
40 additional non- CO_2 controls. To explore this further, we present a multi-proxy (Mg/Ca, $\delta^{18}\text{O}$, TEX_{86})
41 SST record from the western North Atlantic ($\sim 36^\circ\text{N}$ paleolatitude). Our data confirm a long-term
42 decline in SSTs of $\sim 5^\circ\text{C}$ between the early ($\sim 53\text{ Ma}$) and the middle ($\sim 42\text{ Ma}$) Eocene, supporting
43 declining atmospheric CO_2 as the primary mechanism of Eocene cooling. However, from the
44 middle Eocene onwards, North Atlantic zonal temperature gradients are decoupled, which we
45 attribute to the incursion of warmer waters into the eastern North Atlantic and the inception of
46 Northern Component Water across the early-middle Eocene transition.

47

48 **Introduction**

49 The early Eocene Climatic Optimum (EECO; 53.3 to 49.1 million years ago; Ma) (Hollis et al.,
50 2019a) is characterised by a long-term maximum in atmospheric CO_2 ($\sim 1470\text{ ppm}$) (Anagnostou et
51 al., 2020), followed by a gradual decline in atmospheric CO_2 during the middle Eocene (47.8 to
52 38.0 Ma) to $\sim 800\text{ ppm}$ (Anagnostou et al., 2020). This is consistent with declining SSTs in the
53 tropics (ca. 4°C) (Cramwinckel et al., 2018; Evans et al., 2018) and the mid-to-high southern
54 latitudes (ca. $8\text{--}11^\circ\text{C}$; Bijl et al., 2009; Hollis et al., 2009; Hollis et al., 2012). However, SST

55 estimates from the eastern North Atlantic suggest relatively muted surface water cooling ($\sim 1^\circ\text{C}$)
56 between the EECO and middle Eocene (~ 40 Ma) (Bornemann et al., 2016). Temperature
57 asymmetry between the northern and southern hemisphere would not be expected from a long-
58 term decline in atmospheric CO_2 alone (Liu et al., 2018) and suggests that other non- CO_2 driving
59 mechanisms (e.g. gateway reorganisation and/or changes in ocean circulation) may influence
60 regional SST patterns.

61 Of particular relevance is the growing evidence for Northern Component Water (NCW)
62 initiation in the North Atlantic during the early-middle Eocene (~ 47 to 49 Ma) (Boyle et al., 2017;
63 Hohbein et al., 2012; Norris et al., 2001). The onset of NCW has been attributed to gateway
64 reorganisation, specifically deepening of the Greenland-Scotland Ridge (GSR) (Boyle et al., 2017;
65 Hohbein et al., 2012; Vahlenkamp et al., 2018), although other mechanisms have been proposed
66 such as isolation of the Arctic Ocean (Zhang et al., 2011) or restriction of the Tethys Ocean
67 (Roberts et al., 2009). The onset of NCW is followed by a period of weaker overturning (~ 42 to 38
68 Ma) (Witkowski et al., 2021), before re-invigoration of NCW during the late Eocene (~ 38 Ma)
69 (Coxall et al., 2018) or Eocene-Oligocene transition (EOT; ~ 34 Ma) (Hutchinson et al., 2019). The
70 establishment of NCW can transport additional heat into the eastern North Atlantic (Vahlenkamp et
71 al., 2018), potentially muting any long-term cooling trend in this region. This has been invoked to
72 explain stable temperatures in the eastern North Atlantic during the middle Eocene (Bornemann et
73 al., 2016). However, our understanding of long-term North Atlantic temperature change is based a
74 single proxy record (planktonic foraminiferal $\delta^{18}\text{O}$) from a single site (ODP Site 401; Bornemann et
75 al., 2016) and may not be regionally representative.

76 To test whether the wider North Atlantic region exhibits stable temperatures during the
77 Eocene, we use a multi-proxy approach ($\delta^{18}\text{O}$, Mg/Ca, TEX_{86}) to reconstruct SST in the western
78 North Atlantic (Bass River; ODP Leg 174AX; $\sim 36^\circ\text{N}$ paleolatitude) during the early-to-middle
79 Eocene (53.7 to 42.0 Ma). We compare our new dataset with climate model simulations spanning
80 a wide range of CO_2 values to explore (i) temporal and spatial patterns of cooling in the North
81 Atlantic during the Eocene and (ii) whether there is thermal decoupling between the northern and
82 southern hemisphere during the Eocene. This allows us to test whether declining CO_2 is the

83 primary driver of long-term Eocene cooling or whether regional forcing mechanisms are also
84 important.

85 **Methods**

86 *Site description*

87 The Bass River section (ODP Leg 174AX; 39°36'N, 74°26'W) consists of calcareous marls and
88 glauconitic silty clays deposited in middle to outer neritic palaeodepths between 30 and 150 m
89 (Fung et al., 2019; Miller et al., 2003). The biostratigraphic age model was developed using
90 planktonic foraminifera and nannofossils (following Fung et al., 2019) with datums converted to the
91 GTS2012 (Vandenberghe et al., 2012).

92

93 *Analytical methods*

94 Lipid biomarker analysis was performed on 47 sediment samples. Approximately 5-10g of
95 sediment was extracted with an Ethos Ex microwave extraction system using 15 ml of
96 dichloromethane (DCM) and methanol (MeOH) (9:1, v/v). The total lipid extract was separated over
97 silica into apolar and polar fractions using hexane:dichloromethane (9:1, v/v) and
98 dichloromethane:methanol (1:2, v/v), respectively. The polar fraction (containing isoGDGTs) was
99 dissolved in hexane/isopropanol (99:1, v/v), passed through 0.45µm PTFE filters and analysed by
100 HPLC/APCI-MS following Hopmans et al. (2016).

101 Trace element and stable oxygen isotope ($\delta^{18}\text{O}$) planktonic foraminiferal analysis was
102 performed on multiple depth intervals (n = 8) spanning the early-to-middle Eocene. Foraminiferal
103 preservation is excellent, appearing transparent or translucent under the light microscope, with no
104 signs of diagenetic alteration observed under SEM (**Figure S1**). Analysis was performed on
105 various surface-dwelling species (*Acarinina praetopilensis*, *Morozovella formosa*, *Morozovelloides*
106 *crassatus*, and *Pseudohastigerina wilcoxensis*) and deeper, thermocline-dwelling
107 species (*Parasubbotina hagni*, *Parasubbotina inaequispira*). Single-specimen Mg/Ca analysis was
108 performed via laser ablation-inductively coupled mass spectrometry (LA-ICPMS) (see Müller et al.,
109 2009 and Supplementary Information). Mg/Ca values were determined in multiple chambers (~3 to
110 5) within a single specimen and averaged. The same specimens were subsequently analysed for

111 $\delta^{18}\text{O}$ using a Multiprep-Isoprime 100 dual inlet system optimised for analysis of single specimens
112 (Supplementary information).

113 *Temperature calibrations*

114 TEX_{86} data was screened using established indices for non-Thaumarchaeota inputs
115 (Supplementary Information; **Figure S5**) and converted to SST using a Bayesian linear calibration
116 (prior mean = 25, prior standard deviation = 10, $n = 2000$) (Tierney and Tingley, 2014). Planktonic
117 foraminiferal $\delta^{18}\text{O}$ values were converted to SST using the bayfox Bayesian calibration (prior mean
118 = 25, prior standard deviation = 20, $n = 2000$). Seawater $\delta^{18}\text{O}$ values ($\delta^{18}\text{O}_{\text{sw}}$) were defined
119 following the DeepMIP protocols (-1.0‰ ; see Hollis et al., 2019) with a latitude-specific temporal
120 correction following Gaskell et al. (2022). Data (Meckler et al., 2022) and model-based approaches
121 (Gaskell et al., 2022; Zhu et al., 2020) indicate only minor changes in $\delta^{18}\text{O}_{\text{sw}}$ at Bass River location
122 through the early-middle Eocene (e.g., $<0.05\text{‰}$ in between x6 and x3 CO_2 simulations using
123 iCESM1.2).

124 Mg/Ca values were converted to SST using a modified version of MgCaRB (Gray and Evans,
125 2019) (Supplementary Information). We report pH-corrected Mg/Ca temperatures as the majority of
126 modern foraminifer species are characterised by Mg/Ca-pH sensitivity (Gray and Evans, 2019). For
127 Mg/Ca and $\delta^{18}\text{O}$, we report the ‘average’ SST estimates for a given time slice ($n = 8$) by combining
128 (i) multiple-specimens from multiple size fractions and (ii) all surface-dwelling species within
129 multiple genera (i.e., *Acarinina praetopilensis*, *Acarinina pseudotopilensis*, *Morozovella formosa*,
130 *Morozovelloides crassatus*, *Pseudohastigerina wilcoxensis*) into a single estimate, following
131 DeepMIP protocols and adjusting for ODP 174AX sample restrictions (Hollis et al, 2019;
132 Supplementary Information). Average ‘SST’ estimates comprise a minimum of two samples from a
133 single depth horizon (see **Data S4-S5**). When SSTs are calculated using individual species
134 (**Figure S2**) and size segregating species (**Figure S2-S3**), similar patterns in long-term trends are
135 observed.

136

137 *Climate model simulations*

138 We use the isotope-enabled Community Earth System Model version 1.2 (iCESM1.2) (Zhu et al.,
139 2020; Zhu et al., 2019) to compare with our proxy reconstructions and to provide an independent
140 estimate of $\delta^{18}\text{O}_{\text{sw}}$. The iCESM1.2 simulations were performed following the Deep-time Model
141 Intercomparison Project protocols (Lunt et al., 2017) with early Eocene paleogeography and
142 vegetation (56.0–47.8 Ma) (Herold et al., 2014) and atmospheric CO_2 levels of $\times 1$, $\times 3$, $\times 6$, and $\times 9$
143 preindustrial values (284.7 ppmv). Seawater $\delta^{18}\text{O}$ in the simulations was initialized from a constant
144 value of -1.0‰ to account for the absence of ice sheets in a hothouse climate (Hollis et al., 2019).
145 See Zhu et al. (2019; 2020) for further details of the experimental setup, equilibration state, and
146 assessment of the simulation results.

147

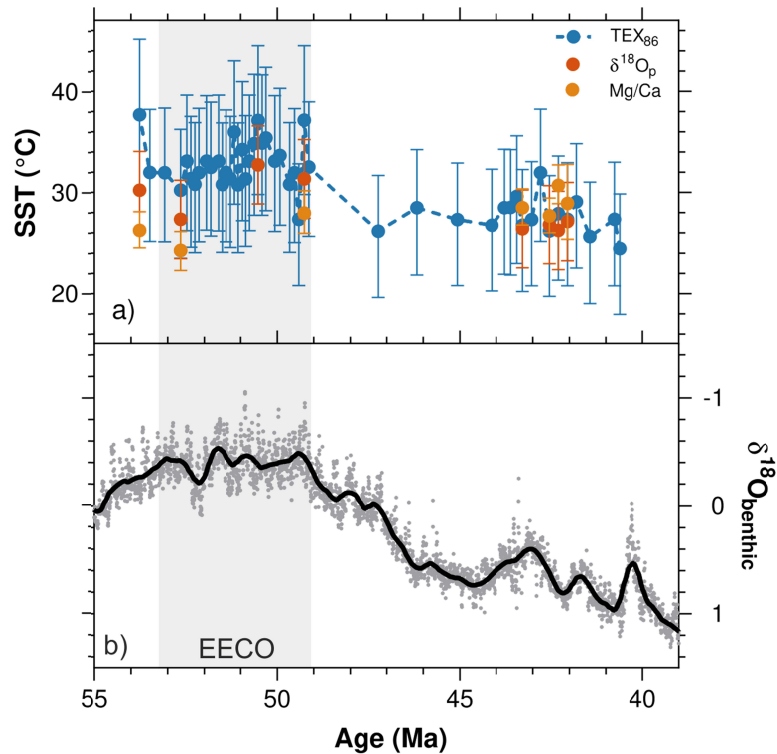


Figure 1. a) SST reconstructions from Bass River during the early-middle Eocene inferred via TEX_{86} (blue), planktonic foraminifera $\delta^{18}\text{O}$ (dark orange) and Mg/Ca (light orange). Error bars represent the 95% confidence intervals. Analytical error for $\delta^{18}\text{O}$ was better than 0.16‰ . **b)** benthic foraminifera $\delta^{18}\text{O}$ values (Westerhold et al., 2020).

148

149 **Results**

150 During the EECO (53.3 to 49.1 Ma), TEX₈₆ SST estimates average ~33°C (**Figure 1a**). Between
151 the EECO and the middle Eocene (~40 Ma), TEX₈₆ SST estimates decline by ~7°C (**Figure 1a**).
152 Oxygen isotope SST estimates during the EECO from surface-dwelling planktonic foraminiferal
153 average ~30°C (**Figure 1a**). Surface-dwelling species yield higher temperatures (~5 to 6°C) than
154 thermocline-dwelling species but exhibit a similar magnitude of cooling (~3°C) between the EECO
155 and the middle Eocene (~42 Ma) (**Figure S3b**). During the early Eocene, Mg/Ca SST estimates
156 (calculated using the *G. ruber* calibration) average ~26°C (**Figure 1a**). These values are lower than
157 δ¹⁸O and TEX₈₆ SST estimates (~30°C and ~33°C, respectively; **Figure 1a**) but agree within the
158 propagated calibration uncertainties. Mg/Ca SST estimates increase by ~3°C between the EECO
159 and middle Eocene (42 Ma; **Figure 1a**). However, the absolute values (~29°C) are comparable to
160 middle Eocene-aged TEX₈₆ and δ¹⁸O SST estimates (28°C and 27°C, respectively) and agree
161 within the propagated calibration uncertainties.

162

163 **Discussion**

164 *Long-term cooling in the western North Atlantic during the Eocene*

165 TEX₈₆ and δ¹⁸O values indicate very high SSTs at Bass River during the EECO (~30 to 33°C).
166 These values are in agreement with existing low-resolution TEX₈₆ estimates generated at Bass
167 River (de Bar et al., 2019) and nearby South Dover Bridge (~34°C; Inglis et al., 2015). Mg/Ca SST
168 estimated are also relatively high (~27°C; **Figure 1**) but are lower than TEX₈₆ and δ¹⁸O-derived
169 SST estimates by ~3-6°C. Between the EECO and middle Eocene (~43-41 Ma), TEX₈₆ and δ¹⁸O
170 values indicate gradual surface water cooling (6 and 3°C, respectively; **Figure 1a**), coherent with
171 declining TEX₈₆ SSTs (~7°C) at South Dover Bridge between the EECO and middle Eocene (~42
172 Ma). Evidence of cooling in multiple proxies and locations provides the first compelling evidence for
173 long-term surface ocean cooling in the (western) North Atlantic between the early and middle
174 Eocene, which is in parallel with the inferred deep-ocean cooling in benthic foraminifera δ¹⁸O
175 record (Figure 1b; Westerhold et al., 2020).

176 In contrast, our new Mg/Ca SSTs increase by $\sim 3^{\circ}\text{C}$ between the EECO and middle
177 Eocene. Although middle Eocene (~ 42 Ma) SST estimates are in excellent agreement with TEX_{86}
178 and $\delta^{18}\text{O}$ values (**Figure 1**) and alkenone-derived SST estimates ($\sim 29\text{-}30^{\circ}\text{C}$; Liu et al, 2018) from
179 nearby site IODP Site 1404, the temporal trends are inconsistent with regional observations (*this*
180 *paper*) (de Bar et al., 2019; Inglis et al., 2015) and declining global bottom water temperature
181 (BWT) estimates inferred via changes in benthic foraminiferal $\delta^{18}\text{O}$ values (Figure 1b) (Westerhold
182 et al., 2020). To explore this mismatch further, we compared our proxy-derived temperature
183 estimates (TEX_{86} , Mg/Ca, $\delta^{18}\text{O}$) alongside iCESM1.2 simulations with different CO_2 scenarios (x1
184 to x9 pre-industrial CO_2) (**Figure 2**). These simulations have previously been shown to replicate
185 key large-scale features of the early Eocene including enhanced global mean surface temperature
186 estimates (Lunt et al., 2021; Zhu et al., 2019), reduced meridional temperature gradients (Lunt et
187 al., 2021), changes in the hydrological cycle (Cramwinckel et al., 2022), and the values and
188 distribution of planktonic foraminifera $\delta^{18}\text{O}$ values (Zhu et al., 2020). iCESM1.2 simulated SST at
189 the Bass River is 30.7 and 26.6°C in the x6 and x3 PI CO_2 simulations, respectively, which
190 overlaps with proxy reconstructions (Figure 2). For a two-fold decrease in atmospheric CO_2 (i.e.,
191 from x6 to x3 PI CO_2), the model predicted decrease in SST of $\sim 4^{\circ}\text{C}$ is comparable to the
192 magnitude of cooling captured by TEX_{86} and $\delta^{18}\text{O}$ (6 and 3°C , respectively; **Figure 2**) between the
193 EECO and middle Eocene, but is inconsistent with warming observed in Mg/Ca values. Given that
194 proxy-derived CO_2 estimates declines from ~ 1470 ppm ($\sim \text{x5}$ PI CO_2) to ~ 800 ppm ($\sim \text{x3}$ PI CO_2)
195 during this interval (Anagnostou et al., 2020), this implies additional non-thermal controls on Mg/Ca
196 values at this site.

197 The choice of Mg/Ca calibration remains uncertain when working with extinct species.
198 However, the discrepancy between Mg/Ca-derived SSTs and other proxy data is insensitive to the
199 choice of Mg/Ca calibration approach (see Supplementary Information). This is because seawater
200 pH was substantially lower than modern throughout the Eocene (Anagnostou et al., 2020), such
201 that choosing a *G. ruber* or *T. sacculifer*-like calibration has a minor effect on the long-term Mg/Ca-
202 derived trend in our dataset (**Figure S4**). Seawater Mg/Ca is also well-constrained for the Eocene

203 (Evans et al., 2018; Gothmann et al., 2015) and is broadly invariant across this interval, such that it
204 is very unlikely that unidentified changes mask cooling. Given that this site was targeted for its
205 exceptional foraminiferal preservation and diverse assemblages (**Figure S1**), this potentially points
206 towards either an evolutionary control on Eocene planktonic foraminifera Mg incorporation, or a
207 shift in seawater carbonate chemistry at this site that substantially differs from the existing pH
208 records (Anagnostou et al., 2020; Rae et al., 2021; see Supplementary Information for more
209 discussion). Resolving this issue and exploring any other additional controls (e.g., local
210 hydrographic variability; c.f. Thornalley et al., 2011) will require further data and is beyond the
211 scope of this study. However, we continue to include the Mg/Ca SST estimates in our assessment
212 of the thermal evolution of the North Atlantic. We also note that this discrepancy may ultimately
213 stem from a small number of Mg/Ca analyses (n=7) from two time slices in the early Eocene
214 (Figure 2), such that this may simply highlight the benefit of working with larger numbers of
215 specimens, where possible.

216

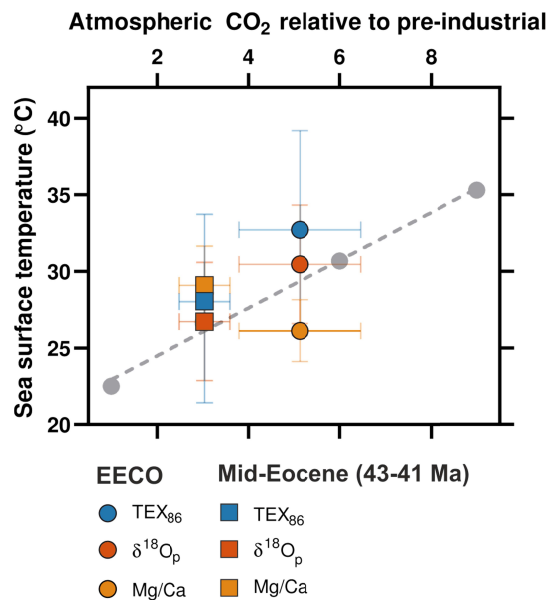


Figure 2: Data-model comparison for Bass River. Grey circles show the CO₂ concentration and sea surface temperature (SST) in the iCESM1.2 simulations (this paper; Zhu et al., 2019).

Dashed line represents a simple linear regression through the model output. Coloured symbols show proxy SST estimates (*this paper*) and CO₂ (Anagnostou et al., 2020) for the EECO (53.3-49.1 Ma; coloured circles) and middle Eocene (43-41 Ma; coloured squares). Error bars represent 90% confidence intervals (SST) or ± 2 standard deviations (CO₂).

217 *Divergent zonal temperature gradients in the North Atlantic during the early-to-middle Eocene*

218 Overall, our new multi-proxy (TEX86, δ¹⁸O, Mg/Ca) results indicate net cooling (~4°C) in the
 219 western North Atlantic between the EECO and middle Eocene (**Figure 1**). Our data from the
 220 western North Atlantic contrasts with existing planktonic foraminifera δ¹⁸O-derived SST estimates
 221 from the eastern North Atlantic (~37° N; ODP Site 401; Bornemann et al., 2016) that indicate
 222 minimal (<1°C) or no cooling between the EECO (ca. 49-50 Ma) and late middle Eocene (ca. 40 –
 223 42 Ma) (**Figure 3a**). The lack of cooling at ODP Site 401 would not be expected from a long-term
 224 decline in atmospheric CO₂. Furthermore, the east-west zonal mean temperature gradient inferred
 225 via proxy estimates (~15-20°C) is much larger than inferred via model simulations (~2~3°C; **Figure**
 226 **3b**) with a range of plausible CO₂ (x1 to x9 pre-industrial CO₂). Collectively, this strongly implies
 227 that other factors influence SSTs in the eastern North Atlantic (ODP Site 401; Bornemann et al.,
 228 2016) during the Eocene.

229

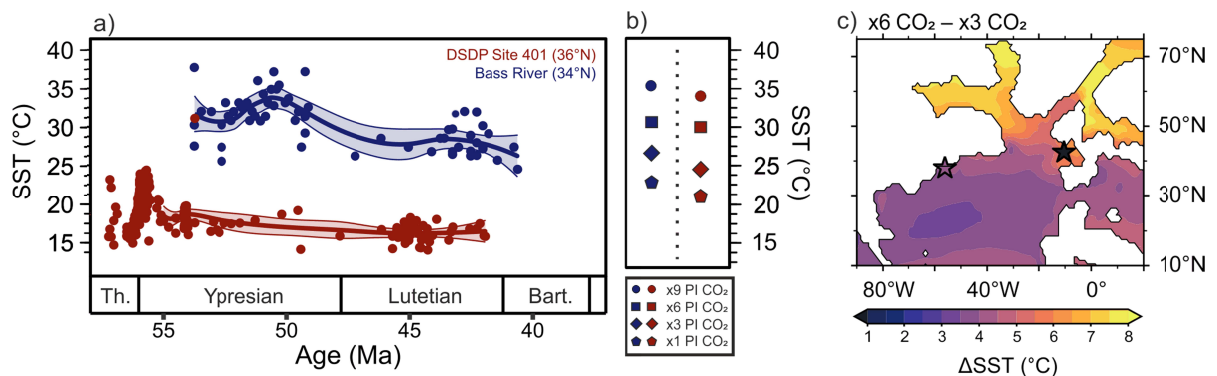


Figure 3: Divergent zonal temperature gradients in the North Atlantic during the early-to-middle Eocene. a) proxy-derived SST reconstructions for Bass River (*this study*) and ODP Site 401 (δ¹⁸O only) (Bornemann et al, 2016) fitted with a LOESS regression. δ¹⁸O values from ODP Site 401 re-

calculated for surface-dwelling foraminiferal genera (*Acarinina* and *Morozovella* spp.) using the bayfox Bayesian calibration ($\delta^{18}\text{O}_{\text{sw}} = -1.0$, prior mean = 25, prior standard deviation = 20, n = 2000). Error bars represent the 95% confidence intervals. b) iCESM1.2-derived SST estimates for Bass River (blue symbols) and ODP Site 401 (red symbols) under different CO_2 concentrations, c) iCESM1.2-derived ΔSST estimates ($\times 6 \text{ PI CO}_2 - \times 3 \text{ PI CO}_2$) with proxy-derived cooling between the early- to middle Eocene shown for each site.

230

231 Planktonic foraminifera at Bass River exhibit excellent preservation (Supplementary
232 Information) and tests are translucent and 'glassy' (**Figure S1**), whereas post-PETM aged
233 planktonic foraminifera at ODP Site 401 exhibit relatively poor preservation (Bornemann et al.,
234 2016) and have been classified as 'recrystallized' (see Hollis al. 2019). However, the influence of
235 diagenesis would act to increase $\delta^{18}\text{O}$ values and overestimate (rather than underestimate) the
236 magnitude of cooling. Therefore, this is unlikely to explain the observed trends (Figure 3).
237 Alternatively, changes in ocean circulation could have modulated regional temperature patterns in
238 the eastern North Atlantic during the middle-to-late Eocene. Recent idealised modelling
239 experiments show that deepening of the Greenland-Scotland Ridge can initiate Northern
240 Component Water (NCW) formation in the North Atlantic and increase SST in the eastern North
241 Atlantic by up to 7°C (Vahlenkamp et al., 2018) and could have muted any long-term CO_2 -driven
242 cooling at ODP Site 401. In contrast, deepening of the Greenland-Scotland Ridge has only a
243 minimal influence ($< 1^\circ\text{C}$) on SSTs in the western North Atlantic (i.e., where Bass River is located)
244 (Vahlenkamp et al., 2018).

245 There is growing geochemical and sedimentological evidence placing the initial onset of
246 NCW between ~ 47 and 49 Ma , coincident with changes in zonal temperature gradients between
247 the eastern and western North Atlantic. Evidence for early onset of NCW between ~ 47 and 49 Ma
248 includes development of contourite drifts in the western North Atlantic (Boyle et al., 2017), changes
249 in biosiliceous sedimentation (Witkowski et al., 2021) and a collapse in $\delta^{13}\text{C}$ gradients between the
250 North and South Atlantic (Hohbein et al., 2012). These changes would also influence local
251 hydrography within the eastern North Atlantic and could exert an additional control on $\delta^{18}\text{O}_{\text{sw}}$

252 values at ODP Site 401. Proxy-based reconstructions during the Middle Eocene Climatic Optimum;
253 have argued that northward expansion of the North Atlantic subtropical gyre could also act as a
254 mechanism to increase SSTs within the North Atlantic (Van Der Ploeg et al., 2023). However,
255 these large-scale regional patterns are not evident in Eocene model simulations and additional
256 proxy data is required to test this further. Thus, we argue that (i) tectonic gateways and changes in
257 ocean circulation may exert a local control on spatial patterns of cooling temperatures, especially in
258 the North Atlantic during the early-to-middle Eocene, and (ii) that diverging zonal temperature
259 gradients in the North Atlantic are consistent with the initial early onset of NCW.

260

261 *Synchronous surface water cooling in the northern and southern hemispheres during the Eocene*

262 Our new multi-proxy SST estimates (**Figure 1**) provide evidence for long-term cooling in the
263 (western) North Atlantic during the middle Eocene. To explore whether long-term cooling is globally
264 synchronous, we compiled early and middle Eocene (56 to 38 Ma) SST estimates from three key
265 regions: (i) the equatorial Atlantic (0-30° N/S) (Cramwinckel et al., 2018; Zhang et al., 2013; Inglis
266 et al., 2015), (ii) the Northwest Atlantic (30-50 °N) (*this study*; de Bar et al., 2019; Inglis et al., 2015;
267 Liu et al., 2018; van der Ploeg et al., 2023) and (iii) the SW Pacific (>50°S) (Bijl et al., 2013; Bijl et
268 al., 2009; Crouch et al., 2020; Hollis et al., 2009; Inglis et al., 2015). (**Figure 4**; see also
269 Supplementary Information).

270 Our results show that the onset of long-term cooling (i.e., post EECO) occurs
271 synchronously around 50-49 Ma in the North Atlantic and SW Pacific (i.e. towards the termination
272 of the EECO; **Figure 4a-c**) and coincides with an increase in the latitudinal SST gradient (**Figure**
273 **4d**). This illustrates that the onset of Eocene cooling is a globally feature and consistent with a
274 decline in atmospheric CO₂ as a forcing mechanism for cooling. During the middle Eocene (~47-42
275 Ma), there is a gradual decrease in the latitudinal SST gradient between the equatorial Atlantic and
276 North Atlantic (**Figure 4d**), implying that NCW formation may have also masked long-term CO₂-
277 driven cooling in the eastern North Atlantic. This can be tested by developing new long-term SSTs
278 records from other regions in the subpolar North Atlantic that could be sensitive to NCW formation
279 (e.g., the Nordic Sea). Alternatively, the magnitude of cooling in the equatorial Atlantic could be

280 exaggerated. Indeed, ODP Site 959 (located in the eastern equatorial Atlantic) is unlikely to be
281 representative of the global tropical ocean signal, because it is located in an area of upwelling, thus
282 physically linked to subsurface waters. There is also evidence for an increase in upwelling during
283 the middle-to-late Eocene at ODP Site 959 which could lead to lower-than-expected SSTs
284 (Cramwinckel et al., 2018).

285 There is also a dramatic decrease in SW Pacific SST estimates ~46-47 Ma (**Figure 4c**) and
286 strengthening of the low-to-high latitude temperature gradient (**Figure 4d**) that is not reflected in
287 either the low- or mid-latitude Atlantic (**Figure 4d**), suggesting additional non-CO₂ controls in the
288 SW Pacific. Previous work argues that the Tasman Gateway was open to shallow circulation at this
289 time (~49 to 46 Ma) (Bijl et al., 2013) and deepening of the Tasman Gateway would initiate
290 regional surface water cooling (Sijp et al., 2011; Sijp et al., 2016) and may account for declining
291 SSTs. Our study reveals that changes in ocean gateways may have influenced spatial patterns of
292 cooling in the North Atlantic (see above) and perhaps also in the SW Pacific (Sijp et al., 2016), but
293 that CO₂ was likely responsible for the majority of long-term Eocene cooling.

294

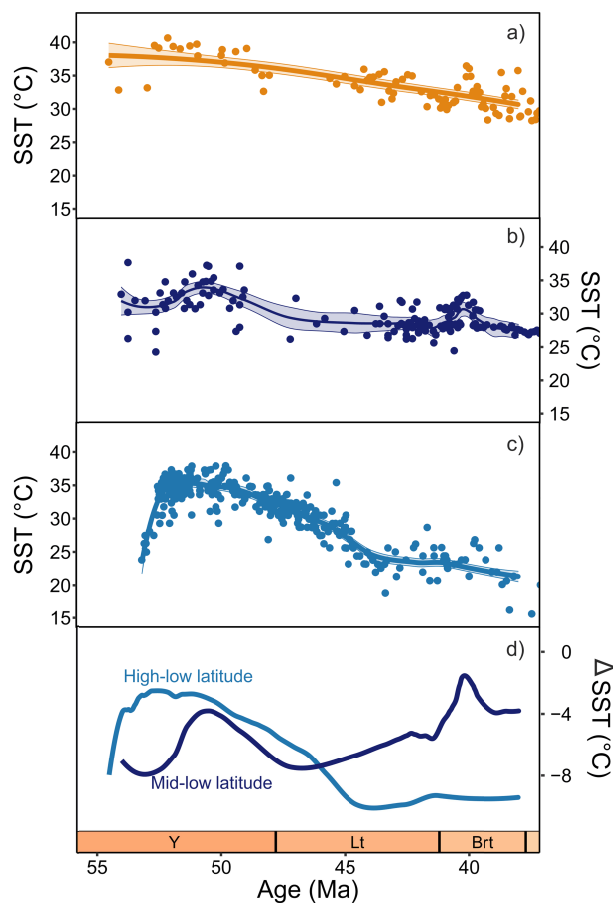


Figure 4: Long-term evolution of surface ocean temperatures during the Eocene in the (a) equatorial Atlantic (Cramwinckel et al., 2018; Inglis et al., 2015; Zhang et al., 2013), b) North Atlantic (this study; Inglis et al., 2015; de Bar et al., 2019), and c) the SW Pacific (Bijl et al., 2013; Bijl et al., 2009; Crouch et al., 2020; Hollis et al., 2009; Inglis et al., 2015). Panel (d) shows the SST gradient between the equatorial Atlantic and the North Atlantic (dark blue line) and SW Pacific (light blue line). To determine the long-term mean SST evolution for the low-, mid-, and high-latitudes, nonparametric LOESS regressions were fitted using the fANCOVA software package (<http://www.R-project.org/>).

295

296 **4 Conclusions**

297 Here we present the first multi-proxy (Mg/Ca, $\delta^{18}\text{O}$, TEX_{86}) SST record from the western North
 298 Atlantic spanning the early-to-middle Eocene. Our results reconstruct very high SSTs during the

299 early Eocene Climatic Optimum (~27-33°C), in agreement with high atmospheric CO₂
300 concentrations. Our multi-proxy results indicate a slow decline (~5°C) in SSTs between the early
301 (~53 Ma) and the middle Eocene (~42 Ma), consistent with long-term decrease in atmospheric
302 CO₂. However, zonal temperature gradients in the North Atlantic are likely decoupled during the
303 early-to-middle Eocene. We attribute this to the inception of Northern Component Water at the
304 early-middle Eocene transition and incursion of warmer waters into the eastern North Atlantic. We
305 demonstrate that the onset of long-term Eocene cooling in the western North Atlantic (~50-49 Ma)
306 occurs synchronously in other ocean basins (e.g., N. Atlantic vs S. Pacific) and across different
307 latitudinal bands. This indicates that CO₂ was likely responsible for the onset of long-term Eocene
308 cooling, but that changes in ocean gateways likely influenced spatial patterns of cooling in different
309 ocean basins, especially during the middle Eocene.

310

311 **Acknowledgements**

312 Samples were provided by IODP which is sponsored by the NSF and participating countries. We
313 thank Jim Browning for information on the age model and Tianchen He for support in trace element
314 and isotope data interpretation. GNI was supported by a Royal Society Dorothy Hodgkin
315 Fellowship (DHF\R1\191178) and NERC (NE/V018388/1). We thank NEIF-B for analytical support
316 and Jim Davy for support with SEM imaging. RB acknowledges funding from a NERC PhD
317 studentship award number 1352360, the Cushman Foundation for Foraminiferal Research (Joseph
318 A. Cushman Award for Student Research), and a 2016 Geologists' Association New Researchers'
319 Award. BW was supported by NERC grants NE/V018361/1 and NE/G014817. LA-ICPMS work at
320 Royal Holloway University of London was partly funded by a 2014 NERC Capital Equipment Grant
321 (Ref: CC073). The CESM project is supported primarily by the National Science Foundation (NSF).
322 This material is based upon work supported by the National Center for Atmospheric Research,
323 which is a major facility sponsored by the NSF under Cooperative Agreement No. 1852977. JZ
324 was supported by NSF Grant 2202777.

325 **Open Research**

326 Inorganic and organic geochemical data is available in the supporting information and at OSF (DOI
327 pending).

328

329 **References**

330 Anagnostou, E., John, E. H., Babila, T., Sexton, P., Ridgwell, A., Lunt, D. J., Pearson, P. N., Chalk,

331 T., Pancost, R. D., and Foster, G., 2020, Proxy evidence for state-dependence of climate

332 sensitivity in the Eocene greenhouse: *Nature Communications*, v. 11, no. 1, p. 1-9.

333 Barker, S., Cacho, I., Benway, H., and Tachikawa, K., 2005, Planktonic foraminiferal Mg/Ca as a

334 proxy for past oceanic temperatures: a methodological overview and data compilation for

335 the Last Glacial Maximum: *Quaternary Science Reviews*, v. 24, no. 7-9, p. 821-834.

336 Bijl, P. K., Bendle, J. A. P., Bohaty, S. M., Pross, J., Schouten, S., Tauxe, L., Stickley, C. E.,

337 McKay, R. M., Röhl, U., Olney, M., Sluijs, A., Escutia, C., Brinkhuis, H., and Scientists, E.,

338 2013, Eocene cooling linked to early flow across the Tasmanian Gateway: *Proceedings of*

339 *the National Academy of Sciences*, v. 110, no. 24, p. 9645-9650.

340 Bijl, P. K., Schouten, S., Sluijs, A., Reichert, G.-J., Zachos, J. C., and Brinkhuis, H., 2009, Early

341 Palaeogene temperature evolution of the southwest Pacific Ocean: *Nature*, v. 461, no.

342 7265, p. 776-779.

343 Bornemann, A., D'haenens, S., Norris, R. D., and Speijer, R. P., 2016, The demise of the early

344 Eocene greenhouse—Decoupled deep and surface water cooling in the eastern North

345 Atlantic: *Global and Planetary Change*, v. 145, p. 130-140.

346 Bornemann, A., Norris, R. D., Lyman, J. A., D'Haenens, S., Groeneveld, J., Röhl, U., Farley, K. A.,

347 and Speijer, R. P., 2014, Persistent environmental change after the Paleocene—Eocene

348 Thermal Maximum in the eastern North Atlantic: *Earth and Planetary Science Letters*, v.

349 394, p. 70-81.

350 Boyle, P. R., Romans, B. W., Tucholke, B. E., Norris, R. D., Swift, S. A., and Sexton, P. F., 2017,

351 Cenozoic North Atlantic deep circulation history recorded in contourite drifts, offshore

352 Newfoundland, Canada: *Marine Geology*, v. 385, p. 185-203.

353 Coxall, H. K., Huck, C. E., Huber, M., Lear, C. H., Legarda-Lisarri, A., O'regan, M., Sliwinska, K. K.,
354 Van De Flierdt, T., De Boer, A. M., and Zachos, J. C., 2018, Export of nutrient rich Northern
355 Component Water preceded early Oligocene Antarctic glaciation: *Nature Geoscience*, v.
356 11, no. 3, p. 190-196.

357 Cramwinckel, M. J., Huber, M., Kocken, I. J., Agnini, C., Bijl, P. K., Bohaty, S. M., Frieling, J.,
358 Goldner, A., Hilgen, F. J., and Kip, E. L., 2018, Synchronous tropical and polar temperature
359 evolution in the Eocene: *Nature*, v. 559, no. 7714, p. 382-386.

360 Crouch, E., Shepherd, C., Morgans, H., Naafs, B., Dallanave, E., Phillips, A., Hollis, C., and
361 Pancost, R. D., 2020, Climatic and environmental changes across the early Eocene climatic
362 optimum at mid-Waipara River, Canterbury Basin, New Zealand: *Earth-Science Reviews*, v.
363 200, p. 102961.

364 de Bar, M., de Nooijer, L., Schouten, S., Ziegler, M., Sluijs, A., and Reichert, G. J., 2019,
365 Comparing seawater temperature proxy records for the past 90 Myrs from the shallow shelf
366 record Bass River, New Jersey: *Paleoceanography and Paleoclimatology*, v. 34, no. 4, p.
367 455-475.

368 Evans, D., Sagoo, N., Renema, W., Cotton, L. J., Müller, W., Todd, J. A., Saraswati, P. K.,
369 Stassen, P., Ziegler, M., and Pearson, P. N., 2018, Eocene greenhouse climate revealed
370 by coupled clumped isotope-Mg/Ca thermometry: *Proceedings of the National Academy of*
371 *Sciences*, v. 115, no. 6, p. 1174-1179.

372 Fung, M. K., Katz, M. E., Miller, K. G., Browning, J. V., and Rosenthal, Y., 2019, Sequence
373 stratigraphy, micropaleontology, and foraminiferal geochemistry, Bass River, New Jersey
374 paleoshelf, USA: Implications for Eocene ice-volume changes: *Geosphere*, v. 15, no. 2, p.
375 502-532.

376 Gaskell, D. E., Huber, M., O'Brien, C. L., Inglis, G. N., Acosta, R. P., Poulsen, C. J., and Hull, P.
377 M., 2022, The latitudinal temperature gradient and its climate dependence as inferred from
378 foraminiferal $\delta^{18}\text{O}$ over the past 95 million years: *Proceedings of the National Academy of*
379 *Sciences*, v. 119, no. 11, p. e2111332119.

380 Gothmann, A. M., Stolarski, J., Adkins, J. F., Schoene, B., Dennis, K. J., Schrag, D. P., Mazur, M.,
381 and Bender, M. L., 2015, Fossil corals as an archive of secular variations in seawater
382 chemistry since the Mesozoic: *Geochimica et Cosmochimica Acta*, v. 160, p. 188-208.

383 Gray, W. R., and Evans, D., 2019, Nonthermal influences on Mg/Ca in planktonic foraminifera: A
384 review of culture studies and application to the last glacial maximum: *Paleoceanography*
385 and *Paleoclimatology*, v. 34, no. 3, p. 306-315.

386 Herold, N., Buzan, J., Seton, M., Goldner, A., Green, J., Müller, R., Markwick, P., and Huber, M.,
387 2014, A suite of early Eocene (~ 55 Ma) climate model boundary conditions: *Geoscientific*
388 *Model Development*.

389 Hohbein, M. W., Sexton, P. F., and Cartwright, J. A., 2012, Onset of North Atlantic Deep Water
390 production coincident with inception of the Cenozoic global cooling trend: *Geology*, v. 40,
391 no. 3, p. 255-258.

392 Hollis, C. J., Dunkley Jones, T., Anagnostou, E., Bijl, P. K., Cramwinckel, M. J., Cui, Y., Dickens,
393 G. R., Edgar, K. M., Eley, Y., and Evans, D., 2019a, The DeepMIP contribution to PMIP4:
394 methodologies for selection, compilation and analysis of latest Paleocene and early Eocene
395 climate proxy data, incorporating version 0.1 of the DeepMIP database: *Geoscientific Model*
396 *Development*, v. 12, no. 7, p. 3149-3206.

397 Hollis, C. J., Dunkley Jones, T., Anagnostou, E., Bijl, P. K., Cramwinckel, M. J., Cui, Y., Dickens,
398 G. R., Edgar, K. M., Eley, Y., Evans, D., Foster, G. L., Frieling, J., Inglis, G. N., Kennedy, E.
399 M., Kozdon, R., Lauretano, V., Lear, C. H., Littler, K., Lourens, L., Meckler, A. N., Naafs, B.
400 D. A., Pälike, H., Pancost, R. D., Pearson, P. N., Röhl, U., Royer, D. L., Salzmann, U.,
401 Schubert, B. A., Seebeck, H., Sluijs, A., Speijer, R. P., Stassen, P., Tierney, J., Tripathi, A.,
402 Wade, B., Westerhold, T., Witkowski, C., Zachos, J. C., Zhang, Y. G., Huber, M., and Lunt,
403 D. J., 2019b, The DeepMIP contribution to PMIP4: methodologies for selection, compilation
404 and analysis of latest Paleocene and early Eocene climate proxy data, incorporating
405 version 0.1 of the DeepMIP database: *Geosci. Model Dev.*, v. 12, no. 7, p. 3149-3206.

406 Hollis, C. J., Handley, L., Crouch, E. M., Morgans, H. E., Baker, J. A., Creech, J., Collins, K. S.,
407 Gibbs, S. J., Huber, M., and Schouten, S., 2009, Tropical sea temperatures in the high-
408 latitude South Pacific during the Eocene: *Geology*, v. 37, no. 2, p. 99-102.

409 Hollis, C. J., Taylor, K. W. R., Handley, L., Pancost, R. D., Huber, M., Creech, J. B., Hines, B. R.,
410 Crouch, E. M., Morgans, H. E. G., Crampton, J. S., Gibbs, S., Pearson, P. N., and Zachos,
411 J. C., 2012, Early Paleogene temperature history of the Southwest Pacific Ocean:
412 Reconciling proxies and models: *Earth and Planetary Science Letters*, v. 349–350, no. 0, p.
413 53-66.

414 Hopmans, E. C., Schouten, S., and Damsté, J. S. S., 2016, The effect of improved
415 chromatography on GDGT-based palaeoproxies: *Organic Geochemistry*, v. 93, p. 1-6.

416 Hutchinson, D. K., Coxall, H. K., O'Regan, M., Nilsson, J., Caballero, R., and de Boer, A. M., 2019,
417 Arctic closure as a trigger for Atlantic overturning at the Eocene-Oligocene Transition:
418 *Nature Communications*, v. 10, no. 1, p. 3797.

419 Inglis, G. N., Farnsworth, A., Lunt, D., Foster, G. L., Hollis, C. J., Pagani, M., Jardine, P. E.,
420 Pearson, P. N., Markwick, P., Galsworthy, A. M. J., Raynham, L., Taylor, K. W. R., and
421 Pancost, R. D., 2015, Descent toward the icehouse; Eocene sea surface cooling inferred
422 from GDGT distributions: *Paleoceanography*, v. 30, no. 7, p. 1000.

423 Inglis, G. N., and Tierney, J. E., 2020, *The TEX86 Paleotemperature Proxy*, Cambridge University
424 Press.

425 Liu, Z., He, Y., Jiang, Y., Wang, H., Liu, W., Bohaty, S. M., and Wilson, P. A., 2018, Transient
426 temperature asymmetry between hemispheres in the Palaeogene Atlantic Ocean: *Nature*
427 *Geoscience*, v. 11, no. 9, p. 656-660.

428 Lunt, D. J., Bragg, F., Chan, W.-L., Hutchinson, D. K., Ladant, J.-B., Morozova, P., Niezgodzki, I.,
429 Steinig, S., Zhang, Z., and Zhu, J., 2021, DeepMIP: Model intercomparison of early Eocene
430 climatic optimum (EECO) large-scale climate features and comparison with proxy data:
431 *Climate of the Past*, v. 17, no. 1, p. 203-227.

432 Lunt, D. J., Huber, M., Anagnostou, E., Baatsen, M. L., Caballero, R., DeConto, R., Dijkstra, H. A.,
433 Donnadiou, Y., Evans, D., and Feng, R., 2017, The DeepMIP contribution to PMIP4:

434 Experimental design for model simulations of the EECO, PETM, and pre-PETM (version
435 1.0): *Geoscientific Model Development*, v. 10, no. 2, p. 889-901.

436 Meckler, A. N., Sexton, P., Piasecki, A., Leutert, T., Marquardt, J., Ziegler, M., Agterhuis, T.,
437 Lourens, L., Rae, J., and Barnet, J., 2022, Cenozoic evolution of deep ocean temperature
438 from clumped isotope thermometry: *Science*, v. 377, no. 6601, p. 86-90.

439 Miller, K., Sugarman, P., and Browning, J., 1. BASS RIVER SITE1.

440 Miller, K. G., Browning, J. V., Sugarman, P. J., McLaughlin, P. P., Kominz, M. A., Olsson, R. K.,
441 Wright, J. D., Cramer, B. S., Pekar, S., and Van Sickel, W., 2003, 174AX leg summary:
442 Sequences, sea level, tectonics, and aquifer resources: *Coastal plain drilling: Proceedings*
443 *of Ocean Drilling Program, Initial Reports, 174AX (Suppl.)*(Ed. by KG Miller, PJ Sugarman
444 & JV Browning, et al.) pp, p. 1-40.

445 Müller, W., Shelley, M., Miller, P., and Broude, S., 2009, Initial performance metrics of a new
446 custom-designed ArF excimer LA-ICPMS system coupled to a two-volume laser-ablation
447 cell: *Journal of Analytical Atomic Spectrometry*, v. 24, no. 2, p. 209-214.

448 Norris, R., Klaus, A., and Kroon, D., 2001, Mid-Eocene deep water, the late Palaeocene thermal
449 maximum and continental slope mass wasting during the Cretaceous-Palaeogene impact:
450 *Geological Society, London, Special Publications*, v. 183, no. 1, p. 23-48.

451 Roberts, C. D., LeGrande, A. N., and Tripathi, A. K., 2009, Climate sensitivity to Arctic seaway
452 restriction during the early Paleogene: *Earth and Planetary Science Letters*, v. 286, no. 3-4,
453 p. 576-585.

454 Sijp, W. P., England, M. H., and Huber, M., 2011, Effect of the deepening of the Tasman Gateway
455 on the global ocean: *Paleoceanography*, v. 26, no. 4.

456 Sijp, W. P., von der Heydt, A. S., and Bijl, P. K., 2016, Model simulations of early westward flow
457 across the Tasman Gateway during the early Eocene: *Climate of the Past*, v. 12, no. 4, p.
458 807-817.

459 Tierney, J. E., and Tingley, M. P., 2014, A Bayesian, spatially-varying calibration model for the
460 TEX₈₆ proxy: *Geochimica et Cosmochimica Acta*, v. 127, p. 83-106.

461 Vahlenkamp, M., Niezgodzki, I., De Vleeschouwer, D., Lohmann, G., Bickert, T., and Pälike, H.,
462 2018, Ocean and climate response to North Atlantic seaway changes at the onset of long-
463 term Eocene cooling: *Earth and Planetary Science Letters*, v. 498, p. 185-195.

464 Van Der Ploeg, R., Cramwinckel, M. J., Kocken, I. J., Leutert, T. J., Bohaty, S. M., Fokkema, C. D.,
465 Hull, P. M., Meckler, A. N., Middelburg, J. J., and Müller, I. A., 2023, North Atlantic surface
466 ocean warming and salinization in response to middle Eocene greenhouse warming:
467 *Science advances*, v. 9, no. 4, p. eabq0110.

468 Westerhold, T., Marwan, N., Drury, A. J., Liebrand, D., Agnini, C., Anagnostou, E., Barnet, J. S.,
469 Bohaty, S. M., De Vleeschouwer, D., and Florindo, F., 2020, An astronomically dated
470 record of Earth's climate and its predictability over the last 66 million years: *Science*, v. 369,
471 no. 6509, p. 1383-1387.

472 Witkowski, J., Bryłka, K., Bohaty, S. M., Mydlowska, E., Penman, D. E., and Wade, B. S., 2021,
473 North Atlantic marine biogenic silica accumulation through the early to middle Paleogene:
474 implications for ocean circulation and silicate weathering feedback: *Climate of the Past*, v.
475 17, no. 5, p. 1937-1954.

476 Zhang, Y. G., Pagani, M., Liu, Z., Bohaty, S. M., and DeConto, R., 2013, A 40-million-year history
477 of atmospheric CO₂: *Philosophical Transactions of the Royal Society A: Mathematical,*
478 *Physical and Engineering Sciences*, v. 371, no. 2001.

479 Zhang, Z., Nisancioglu, K. H., Flatøy, F., Bentsen, M., Bethke, I., and Wang, H., 2011, Tropical
480 seaways played a more important role than high latitude seaways in Cenozoic cooling:
481 *Climate of the Past*, v. 7, no. 3, p. 801-813.

482 Zhu, J., Poulsen, C. J., Otto-Bliesner, B. L., Liu, Z., Brady, E. C., and Noone, D. C., 2020,
483 Simulation of early Eocene water isotopes using an Earth system model and its implication
484 for past climate reconstruction: *Earth and Planetary Science Letters*, v. 537, p. 116164.

485 Zhu, J., Poulsen, C. J., and Tierney, J. E., 2019, Simulation of Eocene extreme warmth and high
486 climate sensitivity through cloud feedbacks: *Science Advances*, v. 5, no. 9, p. eaax1874.

487

Figure 1.

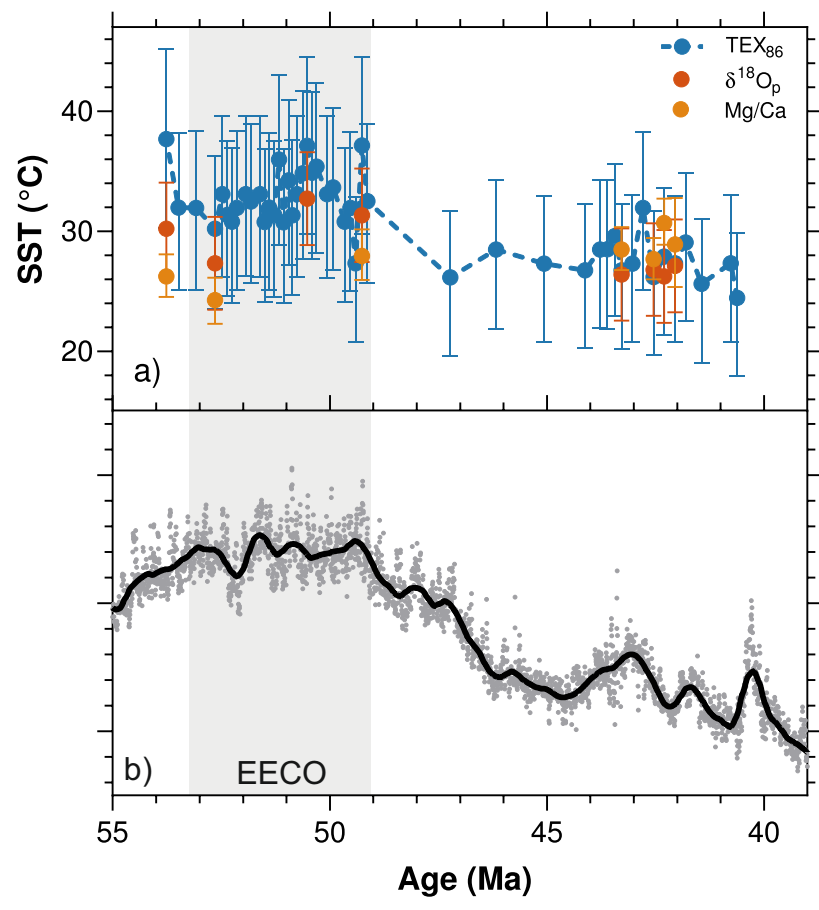
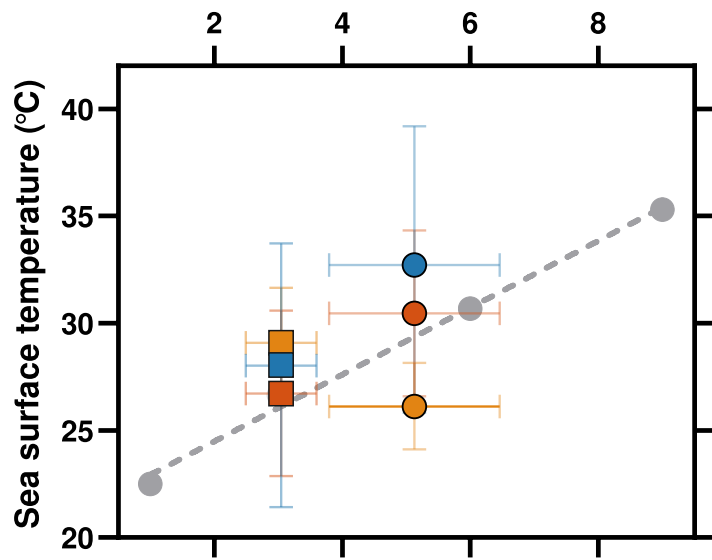


Figure 2.

Atmospheric CO₂ relative to pre-industrial



EECO

Mid-Eocene (43-41 Ma)

● TEX₈₆

■ TEX₈₆

● δ¹⁸O_p

■ δ¹⁸O_p

● Mg/Ca

■ Mg/Ca

Figure 3.

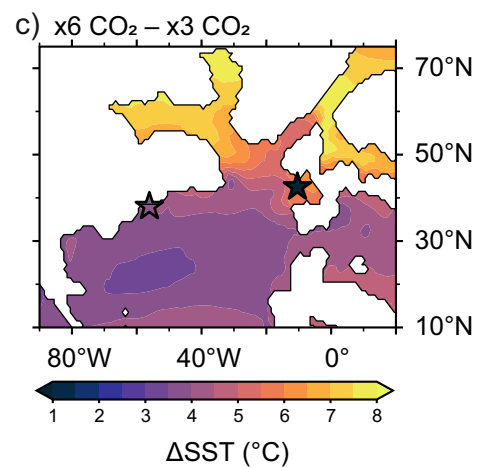
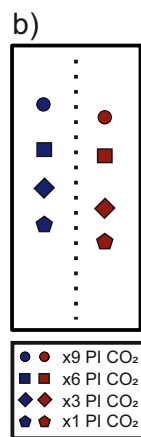
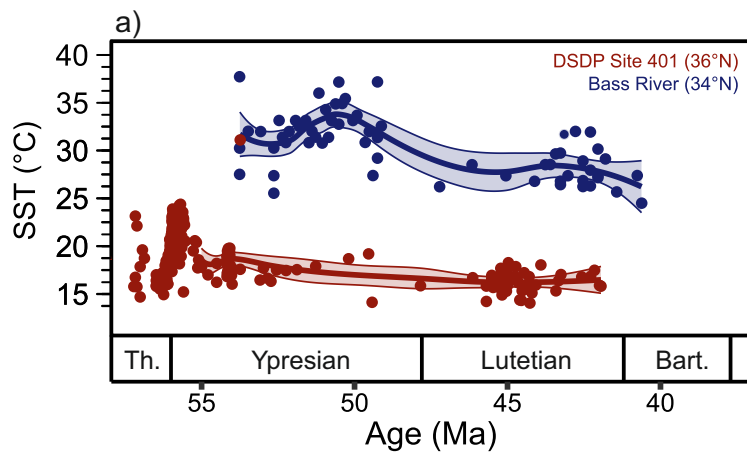


Figure 4.

